Journal of Organometallic Chemistry 694 (2009) 737–746

Contents lists available at ScienceDirect

Journal of Organometallic Chemistry

journal homepage: www.elsevier.com/locate/jorganchem

Synthesis, photophysical and electrophosphorescent properties of mononuclear Pt(II) complexes with arylamine functionalized cyclometalating ligands

Dongfang Qiu [a,b], Jiang Wu [a], Zhiyuan Xie [a], Yanxiang Cheng [a,*], Lixiang Wang [a]

[a] State Key Laboratory of Polymer Physics and Chemistry, Changchun Institute of Applied Chemistry, Chinese Academy of Sciences, 5625 Renmin Street, Changchun, Jilin Province 130022, PR China
[b] Graduate School of Chinese Academy of Sciences, Beijing 100039, PR China

ARTICLE INFO

Article history:
Received 15 September 2008
Received in revised form 27 November 2008
Accepted 2 December 2008
Available online 10 December 2008

Keywords:
Neutral-charge
Platinum
Arylamine
Phosphorescence
Organic light-emitting diode

ABSTRACT

Four cyclometalated Pt(II) complexes, i.e., [($\mathbf{L}^2$)PtCl] (**1b**), [($\mathbf{L}^3$)PtCl] (**1c**), [($\mathbf{L}^2$)PtC≡CC_6H_5] (**2b**) and [($\mathbf{L}^3$)PtC≡CC_6H_5] (**2c**) ($H\mathbf{L}^2$ = 4-[*p*-(*N*-butyl-*N*-phenyl)anilino]-6-phenyl-2,2′-bipyridine and $H\mathbf{L}^3$ = 4-[*p*-(*N*,*N*′-dibutyl-*N*′-phenyl)phenylene-diamino]-phenyl-6-phenyl-2,2′-bipyridine), have been synthesized and verified by ^{1}H NMR, ^{13}C NMR and X-ray crystallography. Unlike previously reported complexes [($\mathbf{L}^1$)PtCl] (**1a**) and [($\mathbf{L}^1$)PtC≡CC_6H_5] (**2a**) ($H\mathbf{L}^1$ = 4,6-diphenyl-2,2′-bipyridine), intense and continuous absorption bands in the region of 300–500 nm with strong metal-to-ligand charge transfer (^{1}MLCT) ($d\pi(Pt) \rightarrow \pi^*(\mathbf{L})$) transitions ($\varepsilon \sim 2 \times 10^4$ dm^3 mol^{-1} cm^{-1}) at 449–467 nm were observed in the UV–Vis absorption spectra of complexes **1b**, **1c**, **2b** and **2c**. Meanwhile, with the introduction of electron-donating arylamino groups in the ligands of **1a** and **2a**, complexes **1b** and **2b** display stronger phosphorescence in CH_2Cl_2 solutions at room temperature with bathochromically shifted emission maxima at 595 and 600 nm, relatively higher quantum yields of 0.11 and 0.26, and much longer lifetimes of 8.4 and 4.5 μs, respectively. An electrochromic film of **1b**-based polymer was obtained on Pt or ITO electrode surface, which suggests an efficient oxidative polymerization behavior. An orange multilayer organic light-emitting diode with **1b** as phosphorescent dopant was fabricated, achieving a maximum current efficiency of 11.3 cd A^{-1} and a maximum external efficiency of 5.7%. The luminescent properties of complexes **1c** and **2c** are dependent on pH value and solvent polarity, which is attributed to the protonation of arylamino units in the C^N^N cyclometalating ligands.

1. Introduction

Cyclometalated platinum(II) complexes have attracted a great deal of attention because of their applications in optoelectronic devices [1–7], chemical sensing [8–10], biochemistry [11] and supramolecular chemistry [12]. Various cyclometalated ligands, such as π-conjugated bidentate [(C^N) motif] [13–22], tridentate phenyl-substituted pyridine [(N^C^N) motif] [23–27] and bipyridine [(C^N^N) motif] [28,29] as well as the related diphenyl-substituted pyridine [(C^N^C) motif] [30–32] systems, have been extensively investigated. Among those, the (C^N^N) tridentate ligands, owning the moderate σ-donating and π-accepting abilities, properly satisfy the demand of the Pt(II) coordination geometry of the square plane to discourage the D_{2d} distortion which is likely to result in a non-radiactive decay [28,33]. Therefore, the corresponding cyclometalated Pt(II) complexes have recently received considerable interest in material science.

At room temperature, cyclometalated Pt(II) complexes are phosphorescent emitting materials with high quantum yields since the strong ligand field effect of the cyclometalated carbon raises the energy of the *d*–*d* states. To fine-tune the emission energy of the (C^N^N) cyclometalated Pt(II) complexes, two main pathways have been exploited by Che's group [34,35]: (1) modification of the substituent in the (C^N^N) ligand. Introduction of the electron-donating group to the bipyridine moiety of the (C^N^N) ligand leads to a hypsochromically shifted emission maximum of Pt(II) complex, while the incorporation of the electron-withdrawing group at the 4-position of the (C^N^N) ligand results in a bathochromic shift of the emission maximum. With the development of the thienyl or furyl moiety as cyclometalating carbon donor, the edge of the MLCT absorption band and the emission maximum substantially red-shift from (C^N^N) to 6-(2-thienyl)-2,2′-bipyridine and 6-(2-furyl)-2,2′-bipyridine ligands. (2) Attachment of acetylide as σ-donor ligand at the fourth coordination site and variation of the substituent in the acetylide moiety. The MLCT absorption band and the emission maximum of the [(C^N^N)PtC≡CC_6H_4-4-R] series systematically red-shift in accordance with the electron-donating ability of the *para*-substituent

* Corresponding author. Tel.: +86 431 85262106; fax: +86 431 85684937 (Y. Cheng).
E-mail addresses: yanxiang@ciac.jl.cn (Y. Cheng), lixiang@ciac.jl.cn (L. Wang).

0022-328X/$ - see front matter © 2008 Elsevier B.V. All rights reserved.
doi:10.1016/j.jorganchem.2008.12.007

in the phenyl-acetylide ligand. The emissive energy of [(C^N^N)Pt-(C≡C)$_n$-R] in CH_2Cl_2 solution at 298 K slightly decreases with the increasing number (n) of ethynyl unit from 1 to 3. Most neutral organometallic complexes are sufficiently stable under sublimation and thus suitable for vacuum deposition in organic light-emitting diodes (OLEDs) fabrication. However, the device efficiencies are unsatisfied due to the low quantum yields (Φ). For example, the orange OLED (λ_{max} = 564 nm; CIE coordinates x = 0.480, y = 0.484) based on [(C^N^N)PtC≡CC$_6$H$_5$] (Φ = 0.04 in CH_2Cl_2) at 4% doping level displays the maximum luminance of 7800 cd m^{-2} at 11 V and the current efficiency of 2.4 cd A^{-1} (η_{ext} = 0.9%) at 30 mA cm^{-2}. And an apparent aggregation-induced quenching effect is observed for further increasing the dopant concentration. Consequently, a new class of Pt(II) complexes with π-conjugated, naphthyl-substituted, and cyclometalating ligands (RC^N^N) was reported [36]. Owing to the high emission quantum yield (Φ = 0.68 in CH_2Cl_2), a yellow OLED (λ_{max} = 536 nm) was fabricated with the maximum luminance of 63 000 cd m^{-2} and the current efficiency of 12.5 cd A^{-1} at 1.8 mA cm^{-2}.

Arylamine and its derivatives are widely utilized as hole-transporting materials in OLEDs [37,20,21], electrochromic polymers [38], and sensitizers in dye-sensitized solar cells (DSSCs) [39–41]. Wang et al. [20,21] integrated hole-transporting triarylamine and electroluminescent [(C^N)Pt(O^O)] component into a single molecule to form one novel multifunctional complex. The bathochromically shifted maxima in the absorption and emission spectra indicate that the incorporation of an electron-rich group, diphenylamine, into the electron-deficient pyridine moiety can strengthen the donor–acceptor (D–A) interaction. However, direct coupling of arylamines with the emissive (C^N^N) cyclometalated Pt(II) complexes has so far never been reported yet. In this paper, four charge-neutral cyclometalated Pt(II) complexes were synthesized by incorporating the *N*-butyl-diphenylamine and *N*,*N*′-dibutyl-*N*,*N*′-diphenyl-1,4-diaminobenzene at the 4-position of the C^N^N ligands (Scheme 1). The fundamental design considerations are: (1) to enhance the charge transfer interaction between the Pt(II) moieties and the ligands; (2) to tune the photophysical properties by changing the electron-donating abilities; (3) to increase their solubility as well as to decrease the intermolecular aggregation. Compared with other reported (C^N^N) Pt(II) complexes, the resulting complexes show unique spectroscopic and electrochemical behaviors. Furthermore, an orange multilayer OLED device with **1b** as phosphorescent material was fabricated and a maximum current efficiency of 11.3 cd A^{-1} with maximum external efficiency (η_{ext}) of 5.7% was achieved. Similar to other charged analogues, complexes **1c** and **2c** illustrate sensitive luminescent spectra which are dependent on acidity and solvent polarity.

2. Results and discussion

2.1. Synthesis and characterization

4,6-Diphenyl-2,2′-bipyridine (H**L**^{1}) and 4-(*p*-bromophenyl)-6-phenyl-2,2′-bipyridine were obtained using Kröhnke's method [42]. In order to facilitate the condensation of aniline or *N*′-(*tert*-butoxycarbonyl)-*N*′-(phenyl)-*p*-phenylenediamine with 4-(*p*-bromophenyl)-6-phenyl-2,2′-bipyridine, the powerful palladium-catalyzed Buchwald method [43] and the efficient Pd(OAc)$_2$/DPE-phos catalyst/ligand system [44] were adopted. To avoid oxidation and improve the solubility, each intermediate amine was protected, in situ, as a *tert*-butyl carbamate (BOC) by adding di-*tert*-butyl bicarbonate ((BOC)$_2$O) and a catalytic amount of 4-(dimethylamino)pyridine (DMAP). The BOC groups were removed quantitatively by thermolysis [45] under an insert atmosphere at 185 °C for 12 h and then reaction with 1-bromobutane afforded arylamino-substituted ligands H**L**^{2} and H**L**^{3}.

The cyclometalated Pt(II) chloride **1b** was synthesized by refluxing the ligand H**L**^{2} and K_2PtCl_4 in CH_3CN/H_2O [34,35] or in glacial acetic acid for 12 h [29]. Using the latter method, complex **1b** was simply obtained in over 90% yield, which is much higher than that (~35%) for the former method. This is probably attributed to the interaction between the arylamino unit and acetic acid which prevents them from coordinating with the metal center. Complex **1c** was synthesized in 84% yield with the same method. Pt(II) acetylide complexes **2a–2c** were obtained by employing Sonogashira's conditions (CuI/Et_3N/CH_2Cl_2) and chromatography separation.

All the cyclometalated Pt(II) complexes have good solubility in CH_2Cl_2 and were verified by ^{1}H NMR, ^{13}C NMR and elementary analysis. Structure of complex **1c** was revealed by X-ray crystallography.

2.2. Crystal structure of complex *1c*

The single crystal of **1c** was grown by slowly evaporating the solvent from its concentrated CH_2Cl_2/MeOH solution. Fig. 1 shows the perspective view and the dimensional packing diagram of **1c**. Selected bond lengths and angles are listed in Table 1. The coordinate geometry of the Pt atom is a distorted square planar configuration with a C(1)–Pt–N(1) angle of 161.6(4)°. The bond distances of Pt–C(1), Pt–N(1) and Pt–N(2) are 1.987(9), 2.091(9) and 1.943(8) Å, respectively, which are comparable to those of previously reported analogous [46–49]. The dihedral angle between the phenyl ring at 4-position of the C^N^N ligand and the plane of the [(C^N^N)Pt] moiety is 33.3°. Interesting intermolecular interactions and conformation are observed in the crystal lattices.

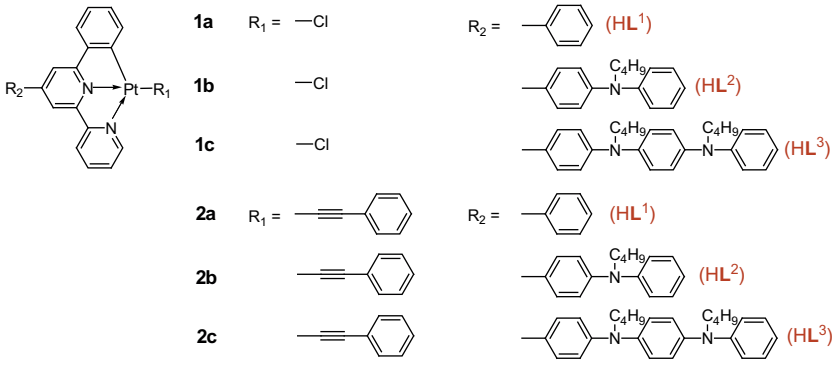

Scheme 1. Schematic structures of the Pt(II) complexes.

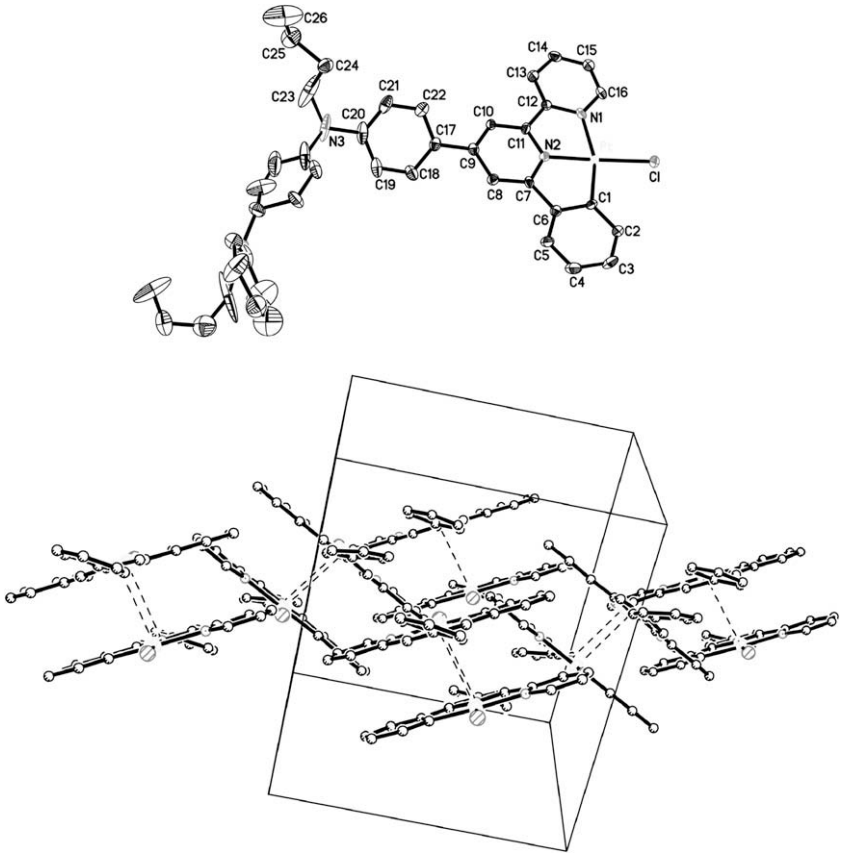

Fig. 1. Perspective view (top) and crystal packing (bottom) of **1c** with the numbering scheme adopted (hydrogen atoms and the Bu-substituted phenylamino units have been omitted for clarity).

Table 1
Selected bond distances (Å) and bond angles (°) for Complex [($\mathbf{L}^3$)PtCl] (**1c**).

Pt–C(1)	1.987(9)	Pt–N(1)	0
Pt–N(2)	1.943(8)	Pt–Cl	2.315(3)
C(1)–Pt–N(1)	161.6(4)	C(1)–Pt–Cl	99.7(3)
C(1)–Pt–N(2)	81.8(4)	N(1)–Pt–Cl	98.7(2)
N(1)–Pt–N(2)	79.8(3)	N(2)–Pt–Cl	178.3(2)

Instead of forming a continuous chain with Pt–Pt linkage in [(C^N^N)PtCl] [48,49], the crystal lattice of **1c** is packed by alternating arranged dimeric [($\mathbf{L}^3$)PtCl] units. The two [($\mathbf{L}^3$)PtCl] units are stacked in a head-to-tail fashion with a Pt–Pt distance of 4.55 Å, suggesting no metal–metal interaction. Furthermore, the interplanar separation of 3.38 Å (C1–C11′) indicates that they are likely to be held together by a weak π–π interaction between the C^N^N ligands.

2.3. UV–Vis absorption spectroscopy

Table 2 summarizes the absorption maxima and extinction coefficients of the absorption bands for the six complexes and Fig. 2 shows the corresponding long-wavelength region of the absorption spectra. The optical spectra of **1a** and **2a** have been described previously [28,35]. Similarly, intense absorption bands in the high-energy region ($\lambda < 376$ nm) with extinction coefficients (ε) of the order of 10^4 L mol^{-1} cm^{-1} were observed in the absorption spectra of **1b**, **1c**, **2b** and **2c**, which are dominated by ^{1}IL ($\pi \rightarrow \pi^*$) transitions, while the low-energy bands with λ_{max} in the range 449–467 nm are assigned to the spin-allowed singlet dπ(Pt) $\rightarrow \pi^*$(L) metal-to-ligand charge transfer (^{1}MLCT) transitions, which are bathochromically shifted and more intense when the complexes change from halides (**1b**, **1c**) to acetylides (**2b**, **2c**). The ^{1}MLCT absorption band obeys Beer's law in the range from 10^{-5} to 10^{-4} mol L^{-1} which might suggests no dimerization or oligomerization of the complexes within this concentration range.

There are some unique features in the absorption spectra of the complexes **1b**, **1c**, **2b** and **2c** (Fig. 2). Firstly, two strong bands are present at around 330 and 375 nm with the absorption intensity increasing over the series **1a–1c** and **2a–2c**. Secondly, with the conjugation of the ligands extending from **1a** to **1c** and **2a** to **2c**, the MLCT absorption bands red-shift gradually, which reflects the lower energetic π^*(L) orbital. Thirdly, most low-energy MLCT bands clearly consist of two overlapping peaks, which suggests that there may be two distinct MLCT transitions, e.g., d_{xz} (Pt) $\rightarrow \pi^*$(L) and d_{yz} (Pt) $\rightarrow \pi^*$(L). And finally, the most interesting point is that the molar extinction coefficients of the MLCT bands are 2–3 times larger than those of the reported C^N^N cyclometalated Pt(II) complexes [34,35].

Table 2
UV–Vis data of the ligands and Pt(II) complexes in CH_2Cl_2 solutions at 298 K.

Compound	λ_{max} (nm)(ε/10^3 dm^3 mol^{-1} cm^{-1})
H$\mathbf{L}^1$	313(14.1), 262(59.6)
H$\mathbf{L}^2$	352(27.7), 289(22.7), 247(35.3)
H$\mathbf{L}^3$	357(27.9), 295(29.5), 247(36.7)
[($\mathbf{L}^1$)PtCl], **1a**	434(4.80), 423(sh,4.65), 368(sh,12.7), 336(21.1), 286(46.4)
[($\mathbf{L}^1$)PtC≡CC_6H_5], **2a**	456(sh,7.53), 444(7.63), 370(sh,13.4), 339(19.0), 286(52.4)
[($\mathbf{L}^2$)PtCl], **1b**	449(20.6), 373(18.6), 327(21.4), 279(33.3)
[($\mathbf{L}^2$)PtC≡CC_6H_5], **2b**	461(sh,23.6), 451(23.8), 376(23.0), 334(24.8), 283(51.8)
[($\mathbf{L}^3$)PtCl], **1c**	459(21.4), 371(18.3), 307(32.1), 295(31.9)
[($\mathbf{L}^3$)PtC≡CC_6H_5], **2c**	467(22.4), 454(sh,21.7), 375(19.1), 325(29.8), 284(46.3)

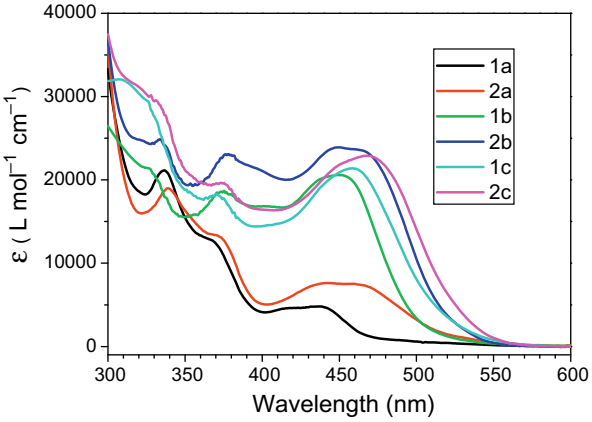

Fig. 2. UV–Vis absorption spectra of the Pt(II) complexes.

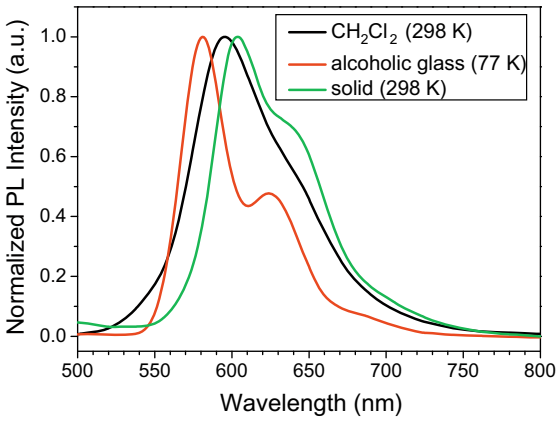

Fig. 3. Normalized PL spectra of **1b** in CH_2Cl_2 (10^{-5} mol L^{-1}) at 298 K, in an alcoholic glass (4:1 EtOH/MeOH) at 77 K and in solid-states at 298 K.

2.4. Photoluminesence (PL) spectroscopy

The PL properties of complexes **1a–1c** and **2a–2c** are listed in Table 3. The maximum PL wavelength, the lifetime and the emission quantum yield of complexes **1a** [28] and **2a** [35] determined in this study are in accordance with the literature results. In CH_2Cl_2 solution, a bathochromic shift of 33 nm and 2 nm, respectively, was observed in the PL spectra of complexes **1b** and **2b** compared with **1a** and **2a**, which is similar to those obtained in the absorption spectra. In addition, the lifetime increases dramatically [from 0.5 (**1a**) to 8.4 (**1b**) μs and 0.9 (**2a**) to 4.5 (**2b**) μs]. The corresponding quantum yields change from 0.07 (**1a**) to 0.11 (**1b**) and 0.11 (**2a**) to 0.26 (**2b**). Complex **2b** demonstrates a PL maximum at 596, 601 and 610 nm in ethanol, CH_2Cl_2 and toluene solutions, respectively. While complex **1b** exhibits a PL maximum at 599, 595 and 592 nm, respectively, in ethanol, CH_2Cl_2 and toluene solutions. This weak and negative solvatochromic effect is ascribed to the polarity difference between the excited states of halide and that of acetylide. At 77 K in alcoholic glass, complexes **1b** and **2b** show well-resolved vibronical emission profile at 540–750 nm and 530–750 nm, respectively (Fig. 3). The large Stoke's shift, long emission lifetime, solvatochromic effect and temperature dependence suggest that the emission of complexes **1b** and **2b** originates from the spin-forbidden triplet excited state. With reference to **1a** and **2a**, the ^{3}MLCT of **1b** and **2b** shifts to the lower energy region. This reveals that the lower π^*(L) energy level of the arylamine functionalized C^N^N ligand decreases the ^{3}MLCT energy gap. Complexes **1b** and **2b** exhibit PL maxima at 604 nm (Fig. 3) and 591 nm, respectively, in solid-states at 298 K. The relatively small bathochromically shifted bands indicate no MMLCT emission arises from Pt–Pt interaction.

Complexes **1c** and **2c** demonstrate weak emissions in alcoholic glass and solid-states, and no apparent emission can be observed in CH_2Cl_2 solutions at 298 K. With reference to earlier work [30,50], this indicates an additional non-radiative decay pathway, namely PET (photo-induced electron transfer), occurs in complexes **1c** and **2c**. The bis-arylamino unit in each of them acts as an electron donor to quench the radiative pathway. Moreover, the strong emissions are resumed in acidic media for both [λ_{max} = 578 nm for **1c** (Fig. 4) and λ_{max} = 615 nm for **2c**], which is due to the proton-induced suppression of the PET process [30].

The pH dependence of complex **1c** was also studied by investigating the influences of various inorganic and organic acids, such as $HClO_4$, HCl, H_2SO_4, CF_3COOH and $CH_3C_6H_4SO_3H$. Among these, $HClO_4$ has the largest protonation effect, which is likely attributed to its strong acidity and good compatibility with the organic solvent. Continuous acid titration was performed in CH_2Cl_2/EtOH system with a complex concentration of 1.0×10^{-5} mol L^{-1}. Fig. 5 shows the relationship between the emission intensity (λ_{max} = 578 nm) of complex **1c** and $HClO_4$ concentration. The emission intensity at 578 nm gradually increases with the $HClO_4$ concentration increasing, which reflects that the amine receptor becomes completely protonated and quenching of the excited state is precluded. Such a protonation of the amino unit is further proved by the change in the absorption spectrum of complex **1c** with the titration of $HClO_4$ (Fig. 6). A broad and weak absorption band at

Table 3
PL data of the ligands and Pt(II) complexes.

Compound	λ_{max} (nm) (τ/μs; Φ[b]) in fluid solution[a]	λ_{max} (nm) in alcoholic glass[c]	λ_{max} (nm) in solid-states (298 K)
HL[1]	358		
HL[2]	409		
HL[3]	403		
1a	562(0.5; 0.07)	545, 586	624, 741
2a	598(0.9; 0.11)	541, 580(sh)	607
1b	595(8.4; 0.11)	581, 624	604, 625(sh)
2b	600(4.5; 0.26)	576, 618	591, 604(sh)
1c	No emission	588, 616(sh)	603
2c	No emission	583, 615(sh)	608, 631(sh)

[a] Measured in degassed CH_2Cl_2 solutions at 298 K (concentration ~ 1×10^{-5} mol dm^{-3}).
[b] $[Ru(bpy)_3](PF_6)_2$ in degassed acetonitrile at 298 K (Φ_r = 0.062) as reference.
[c] Measured in CH_3OH/C_2H_5OH = 1/4 (V/V) at 77 K.

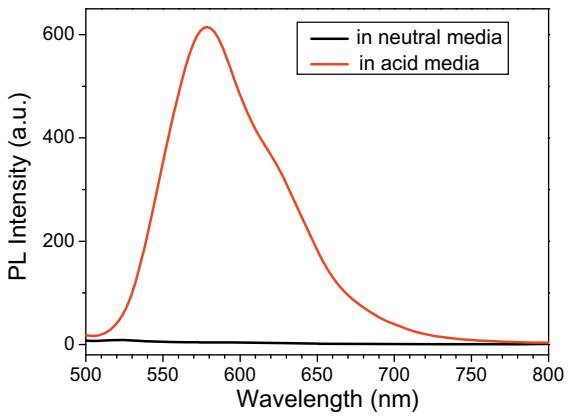

Fig. 4. PL spectra of **1c** in neutral CH_2Cl_2 solutions and in the acidified CH_2Cl_2/EtOH solutions at 298 K.

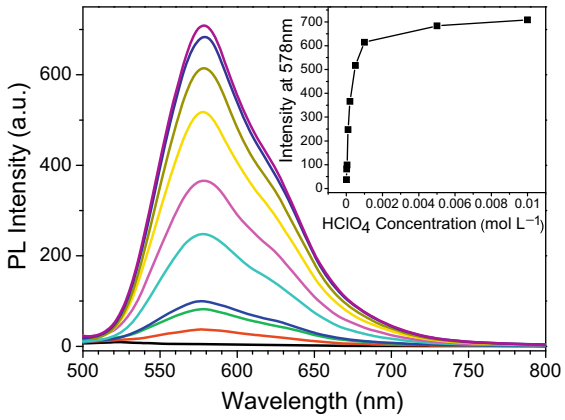

Fig. 5. Influence of $HClO_4$ concentration on the PL spectra for **1c** (10^{-5} mol L^{-1}) in CH_2Cl_2/EtOH solutions (from bottom: 0, 10^{-5}, 2×10^{-5}, 5×10^{-5}, 10^{-4}, 2×10^{-4}, 5×10^{-4}, 10^{-3}, 5×10^{-3}, 10^{-2} mol L^{-1}; λ_{ex} = 450 nm). The inset shows the plots of the PL intensity at 578 nm vs. the $HClO_4$ concentration.

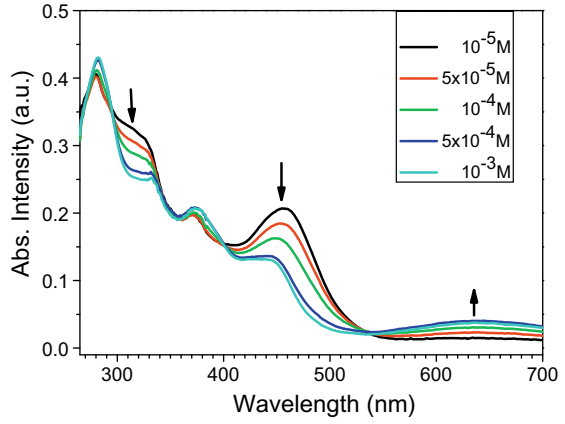

Fig. 6. Influence of $HClO_4$ concentration on the UV-Vis absorption spectra for **1c** (10^{-5} mol L^{-1}) in CH_2Cl_2/EtOH solutions (from top: 10^{-5}, 5×10^{-5}, 10^{-4}, 5×10^{-4}, 10^{-3} mol L^{-1}).

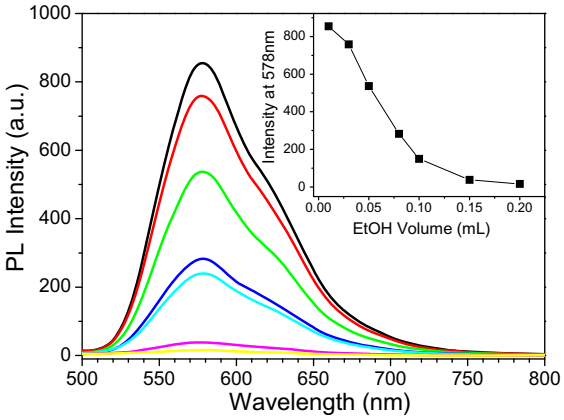

Fig. 7. Influence of EtOH volume on the PL spetra for **1c** in CH_2Cl_2/EtOH solutions (concentrations of **1c** and $HClO_4$ are 10^{-5} and 10^{-4} mol L^{-1}, respectively; from top: 0.01, 0.03, 0.05, 0.08, 0.10, 0.15, 0.20 mL; λ_{ex} = 450 nm). The inset shows the plots of PL intensity at 578 nm vs. the EtOH volume.

Table 4
Electrochemistry data[a] of the ligands and Pt(II) Complexes.

Compound	Oxidation, $E_{p,a}$ (V)[b]		Reduction $E_{1/2}$ (V)[b]	HOMO[c] (eV)	LUMO[c] (eV)	Eg (eV)
	Ligand-based	Metal-based				
HL^1	–			−6.0	−2.6	2.4
HL^2	+0.59			−5.2	−2.8	2.4
HL^3	+0.03, +0.55			−4.7	−2.7	2.0
1a	–	+0.39	−1.77	−5.1	−3.1	2.0
2a	–	+0.41	−1.79	−5.0	−3.1	1.9
1b	+0.57	+0.49(sh)	−1.85	−5.1	−3.1	2.0
2b	+0.62	+0.47(sh)	−1.82	−4.9	−3.1	1.8
1c	+0.06, +0.53	+0.42(sh)	−1.84	−4.7	−3.1	1.6
2c	+0.06, +0.51	Overlapped	−1.86	−4.7	−3.1	1.6

[a] Determined in CH_2Cl_2 at 298 K with 0.1 mol dm^{-3} $^nBu_4NClO_4$ as supporting electrolyte; scanning rate: 100 mV s^{-1}.
[b] Values are reported vs. Fc^+/Fc [$E_{1/2}$ = +0.49 V vs. saturated calomel electrode (SCE)].
[c] Calculated from the onset value of the first oxidation wave in the anodic segment and the reduction wave in the cathodic segment of the CV spectrum.

long-wavelength region is present, which is usually observed for the protonation of oligoanilines [39]. A well defined isosbestic point at 533 nm indicates a clean conversion between the protonated and deprotonated forms. The intensity of the MLCT band decreases with a hypsochromically shifted absorption maximum. Meanwhile, a solvent polarity dependence was also observed. Generally, increasing the solvent polarity, by adding another more polar solvent, or increasing the fraction of the polar solvent (Fig. 7) leads to an efficient solvent-induced quenching of complexes **1c** and **2c**, which is probably ascribed to the intermolecular stacking in the mixed solvent.

2.5. Electrochemistry

The electrochemical behaviors of the ligands and Pt(II) complexes were investigated by cyclic voltammetry (CV) and the data are listed in Table 4. In general, each CV curve exhibits one reversible reduction couple with $E_{1/2}$ in the range −1.77 to −1.86 V vs. $Cp_2Fe^{+/0}$, which presumably corresponds to the one-electron reduction of the C^N^N ligand [35]. The electro-donating arylamino groups in **1b, 1c**, **2b** and **2c** shift the reduction waves to more negative direction. The oxidation potential of the 4-phenyl-substituted C^N^N ligand (HL^1) is beyond the potential window of the solvent, therefore no oxidation peak could be observed. The CV spectrum shows single oxidation peak at +0.59 V for HL^2, according to forming a radical cation species arising from the loss of a single electron in the arylamino unit [51]. For ligand HL^3 with a bis-arylamino unit, two oxidation peaks are present at +0.03 and +0.55 V, which involve two consecutive one-electron transfer processes to form a di(cation radical) species [52]. In the CV spectra of the Pt(II) complexes, the irreversible metal-based oxidation waves at +0.39 and +0.41 V are observed for **1a** and **2a**, respectively. Due to overlapping with those of the arylamino units, the oxidation waves of metal center are present as shoulder peaks for **1b, 1c** and **2b**, while no obvious peak is observed for **2c**.

The energy levels of ligands and complexes are also listed in Table 4. Generally, the Eg decreases gradually over the series **1a**–**1c** and **2a**–**2c**, which arises from the decrease of the HOMO value but no change of the LUMO level, according with the absorption studies.

2.6. Electropolymerization of *1b*

Continuous cycling of the working Pt or indium tin oxide (ITO) electrode with potential from 0 to 1.8 V in a 0.5 mM solution of **1b** resulted in the formation of an orange-brown adherent film on the electrode surface. Fig. 8 shows the repetitive cyclic

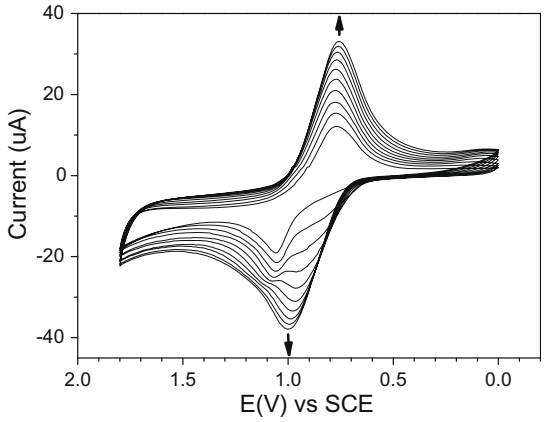

Fig. 8. Repetitive cyclic voltammograms of **1b** on a Pt electrode.

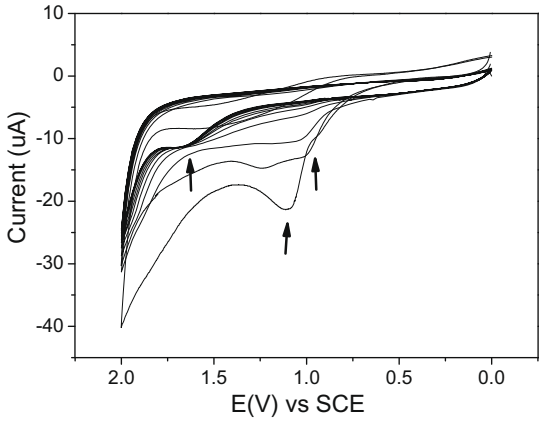

Fig. 10. Repetitive cyclic voltammograms of **2b** on a Pt electrode.

voltammograms of **1b** on a Pt electrode. As the cyclic scan proceeding, the oxidation wave of metal center at +0.98 V vs. SCE considerably increases and shifts to positive potential and finally combines with the arylamine oxidation wave at +1.06 V. Both anodic and cathodic currents increase with scan number, clearly indicating that the deposited film is conductive. The electrochromic film is orange-brown in the neutral state, and is black when fully oxidized. Due to the insolubility of the film, further characterization by either NMR or MS methods is unsuccessful. Since the two oxidation waves overlap seriously, it is difficult to further study the polymerization mechanism by selective oxidation. But it is believed that the radical cation species, resulting from the oxidation of amino unit, triggers the polymerization process and the $[(C^N^N)Pt]^+$ core plays a key role in the stabilization of the radical cation species [53–57].

To investigate the effect of oxidation on the spectral characteristics of the electropolymerized film, the spectroelectrochemistry of poly-**1b** film on a transparent ITO electrode was carried out. The CV of **1b** on the ITO electrode is similar to that obtained on a Pt electrode, although the positions of all the waves shift to positive direction due to the resistance of the ITO layer. The optical spectra of the film were collected at three potentials: reduced at 0 V, partially oxidized at +1.0 V, and fully oxidized at +1.4 V. The spectra over the region of 300–1500 nm are shown in Fig. 9. When the potential is 0 V, the reduced film shows two strong bands at 335 and 462 nm, which are assigned to the ^{1}IL ($\pi \rightarrow \pi^*$) transition and the spin-allowed singlet $d\pi(Pt) \rightarrow \pi^*(L)$ metal-to-ligand charge transfer (^{1}MLCT) transition. Upon oxidation of the film at 1.0 V, the polymer undergoes a color change to dark-blue and several

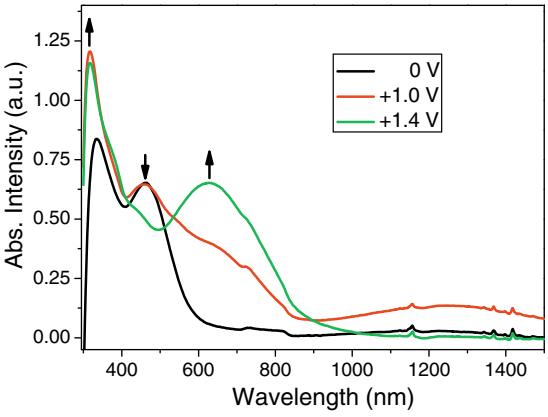

Fig. 9. Spectroelectrochemical spectra of electropolymer **1b**-coated ITO.

changes are observed in the spectra. The absorption band at 335 nm slightly blue-shifts with considerably increased intensity. Additionally, a shoulder band at around 630 nm and a weak but broad band at 1250 nm are present. The NIR band is associated with the appearance of free carriers in the highly conductive state of purely organic conducting polymers or their hybrids [54]. Fully oxidation at +1.4 V results in a sharp decrease in the intensity of the high-energy absorption band at 462 nm, along with the disappearance of the NIR absorption band centered at 1250 nm and the formation of the broad band in the region of 450–1000 nm.

The CV behavior of **2b** is expected to be similar to that of **1b** due to their similar chemical structure. However, two irreversible oxidation waves based on the metal center and the arylamino units are present at the first circle scan (Fig. 10). Both of them considerably decrease and shift to positive potentials with the scan number increasing. After several circle scans, only a weak oxidation wave at +1.7 V is observed. No obvious film deposited on the Pt electrode surface is obtained.

2.7. Electrophosphorescence

To investigate the electrophosphorescent properties of complexes **1b** and **2b**, multilayer OLEDs with configuration reported by Chi-Ming Che [35] were fabricated. Unfortunately, due to the serious decomposition during vacuum deposition, the device based on complex **2b** was not fabricated successfully, while the devices incorporating complex **1b** were prepared and their performance was systematically studied by optimizing the thickness of hole-transporting α-napthylphenylbiphenyl diamine (NPB) and exciton-blocking 2,9-dimethyl-4,7-diphenyl-1,10-phenanthroline (BCP) layers, and the emitter doping level in the host of carbazole biphenyl (CBP). The data of OLEDs performance are listed in Table 5. Generally, thinner NPB layer (40 nm) and lower doping ratio (1%) resulted in a weak emission from CBP at around 440 nm, while thicker NPB layer (80 nm) led to a lower efficiency. The optimum device configuration of ITO/NPB (60 nm)/CBP: 9 wt% of **1b** (30 nm)/BCP (20 nm)/Alq_3 (20 nm)/LiF (1 nm)/Al was obtained and its voltage–current–luminance and current-external quantum efficiency curves were shown in Fig. 11. This OLED shows an efficient orange emission with emission peak at 588 nm and CIE coordinates of (0.570, 0.427) and the EL spectrum shows no apparent voltage-dependence from 6 V to 10 V. The device turns on at 4.0 V and a luminance of 9000 cd m^{-2} is achieved at 13 V. The maximum luminous efficiency is about 11.3 cd A^{-1} and the corresponding external quantum efficiency is 5.7%. Clearly, the performance of this OLED device is significantly better than those of other reported (C^N^N) cyclometalated Pt(II) complexes, and

Table 5
Electrophosphorescence data of complex **1b**.

No.	NPB (nm)	*x*%**1b** in CBP	BCP (nm)	Turn-on voltage (V)	Maximum brightness (cd m^{-2})	Maximum efficiency (cd A^{-1})
1	40	6	10	4.0(1.9)[a]	8417(12.0 V)	8.1
2	60	6	10	4.0(12.5)[a]	10450(9.7 V)	8.9
3	80	6	10	4.0(2.3)[a]	8116(12.4 V)	7.4
4	60	1	10	3.8(1.1)[a]	9909(11.0 V)	6.4
5	60	3	10	4.0(3.1)[a]	10250(10.0 V)	7.9
6	60	9	10	4.0(1.3)[a]	10580(10.9 V)	8.9
7	60	9	20	4.2(1.7)[a]	9045(13.2 V)	11.3
8	60	9	30	4.5(10.9)[a]	9304(12.5 V)	10.6

[a] The brightness (cd m^{-2}) of OLEDs at the corresponding turn-on voltage (V).

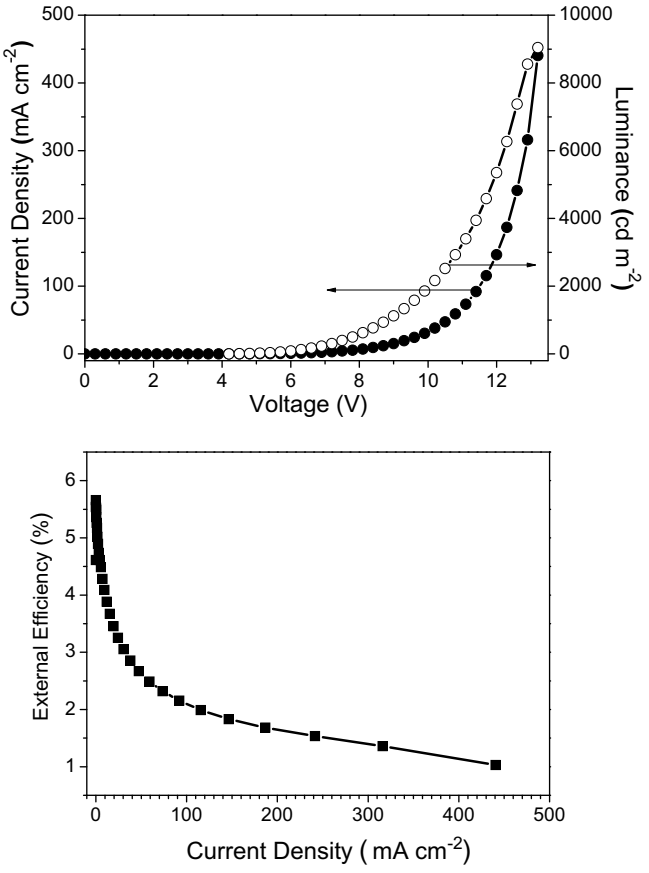

Fig. 11. Current density–voltage and luminance–voltage (top) and external quantum efficiency-current density (bottom) plots for the multilayer OLED based on **1b**.

the current efficiency of this device is comparable to that of the (RC^N^N) cyclometalated Pt(II) complexes [36]. The outstanding performance is probably attributed to the higher emission quantum yield, the longer lifetime of the excited state and the better charge transfer property of the arylamino moiety.

3. Conclusions

In summary, the four bis-component cyclometalated Pt(II) complexes were successfully synthesized by incorporating arylamino units at the 4-position of the C^N^N ligand. As electron donors, the arylamino units strengthen the D–A interaction in all complexes, resulting in intense and continuous bands (300–500 nm) in the absorption spectra. Furthermore, compared with other reported (C^N^N) cyclometalated Pt(II) complexes without the arylamino unit, complexes **1b** and **2b** display strong phosphorescence at 298 K in CH_2Cl_2 solutions with red-shifted emission maxima, higher quantum yields, and longer lifetimes. An orange multilayer OLED device with **1b** as phosphorescent dopant was fabricated with a maximum current efficiency of 11.3 cd A^{-1} and a maximum external efficiency of 5.7%. However, the incorporation of the bis-arylamino units in complexes **1c** and **2c** results in luminescence quenching due to a PET process. Moreover, the luminescence of complexes **1c** and **2c** illustrates sensitive dependence on pH value since the protonation of the bis-arylamino units depress the PET process.

4. Experimental

4.1. General procedures

Melting points were recorded on a hot stage apparatus and are uncorrected. ^1H and ^{13}C NMR spectra were recorded on Bruker AV 300 spectrometers and referenced with respect to TMS internal standard. Elemental analyses were carried out using a Bio-Rad Co's elemental analytical instrument. UV–Vis absorption spectra were obtained using a Perkin–Elmer UV-35 spectrophotometer. PL spectra were performed on a Perkin–Elmer LS50B spectrometer. CV spectra were conducted on a EG&G 283 electrochemical workstation in CH_2Cl_2 solutions with a three-electrode electrochemical cell using Pt electrode, SCE and Pt wire as the working electrode, the reference and counter electrode, respectively. $^nBu_4NClO_4$ (0.1 mol L^{-1}) was used as the supporting electrolyte and the scan rate was 100 mV s^{-1}.

Reactions under argon atmosphere were carried out in oven-dried glassware using standard Schlenk techniques. THF was distilled under argon from sodium benzophenone ketyl. Toluene was distilled under argon from molten sodium. All other solvents were analytical reagent grades and used as supplied.

All the reagents were analytical grades. *p*-Aminodiphenylamine, benzophenone, palladium acetate ($Pd(OAc)_2$), sodium *tert*-butoxide ($NaOBu^t$) (Acros), bis[(2-diphenylphosphino)phenyl]ether (DPEphos, Acros), di-*tert*-butyl bicarbonate ($(BOC)_2O$) (1.0 M in THF) (Acros), 4-(dimethylamino)pyridine (DMAP, Acros), palladium on carbon (Pd/C, 10%), ammonium formate, 2-acetylpyridine, 4-bromo-phenylaldehyde, NaH (>52%, in mineral oil), *n*-bromobutane were all used as received without further purification.

4-Phenyl-6-phenyl-2,2′-bipyridine (H**L**[1]) [28] and *N*′-(*tert*-butoxycarbonyl)-*N*′-(phenyl)-*p*-phenylenediamine [58] were synthesized according to literature methods.

4.2. Preparations of ligands

4.2.1. Synthesis of 4-(p-bromophenyl)-6-phenyl-2,2′-bipyridine

4-(*p*-Bromophenyl)-6-phenyl-2,2′-bipyridine was synthesized according to the literature method [42] and recrystallized twice to form white needles: 4.5 g (36%). M.p.: 153–154 °C. ^1H NMR (300 MHz, $CDCl_3$): δ 8.73–8.67 (m, 2H), 8.61 (s, 1H), 8.20 (d,

J = 9.6 Hz, 2H), 7.93 (s, 1H), 7.87 (t, J = 7.7 Hz, 1H), 7.71–7.63 (m, 4H), 7.56–7.46 (m, 3H), 7.35 (t, J = 6.2 Hz, 1H, Ar). ^{13}C NMR (75 MHz, $CDCl_3$): δ 157.7, 156.8, 156.5, 149.5, 149.4, 139.7, 138.1, 137.3, 132.6, 129.6, 129.2, 127.5, 124.3, 123.8, 121.9, 118.5, 117.5 (Ar). GC–MS: 386. Anal. Calc. for $C_{22}H_{15}BrN_2$: C, 68.23; H, 3.90; N, 7.23. Found: C, 68.20; H, 3.69; N, 7.05%.

4.2.2. Synthesis of ligand H**L²**

4-(*p*-Bromophenyl)-6-phenyl-2,2′-bipyridine (3.87 g, 10.0 mmol), palladium acetate (25.0 mg, 0.11 mmol) and DPEphos (87.0 mg, 0.16 mmol) were charged into a flask and purged with argon. Aniline (1.4 mL, 15.0 mmol) was added via syringe, followed by toluene (40 ml). NaOBu^t (1.62 g, 16.9 mmol) was added in one portion. The reaction mixture was heated to 80 °C under stirring for 9 h. The solvent was removed by rotary evaporation. The residue was dissolved in dichloromethane, washed with distilled water, and dried over anhydrous sodium sulfate and concentrated.

The residue was dissolved in THF (100 mL). NaH (4.82 g, >52%, in mineral oil) was added and purged with argon. The reaction mixture was stirred for 1 h at room temperature, and then 1-bromobutylane (4.0 mL, 40.0 mmol) was added dropwise via syringe. After the solution was refluxed until the conversion was complete (as monitored by thin layer chromatography), it was cooled to room temperature and poured into ice-water mixture slowly, extracted with CH_2Cl_2 until the water phase was colorless. The combined organic solutions were washed with distilled water, dried over anhydrous sodium sulfate and concentrated. The crude product was purified by column chromatography [silica gel, petroleum ether (PE):CH_2Cl_2 = 5:1 (V/V) to CH_2Cl_2:PE = 3:1 (V/V)]. Ligand H**L²** was obtained as white needle crystal by recrystallizing from MeOH/ethyl acetate (EA) solution: 3.9 g (yield: 86%). M.p.: 118–119 °C. ^{1}H NMR (300 MHz, $CDCl_3$): δ 8.72–8.67 (m, 2H), 8.62 (s, 1H), 8.20 (d, J = 8.5 Hz, 2H), 7.95 (s, 1H), 7.86 (t, J = 8.6 Hz, 1H), 7.73(d, J = 8.8 Hz, 2H), 7.55–7.45 (m, 3H), 7.39–7.32 (m, 3H), 7.18–7.11 (m, 3H), 6.98 (d, J = 8.8 Hz, 2H, Ar), 3.76 (t, J = 7.6 Hz, 2H, α (–CH_2)), 1.70 (m, 2H, β (–CH_2)), 1.42 (m, 2H, γ (–CH_2)), 0.96 (t, J = 7.4 Hz, 3H, –CH_3). ^{13}C NMR (75 MHz, $CDCl_3$): δ 157.0, 156.7, 156.1, 149.8, 149.2, 149.0, 147.4, 139.8, 136.8, 129.6, 128.9, 128.7, 128.0, 127.1, 124.2, 123.7, 123.5, 121.5, 117.8, 117.5, 116.6 (Ar), 52.2 (α-CH_2), 29.7 (β-CH_2), 20.3 (γ-CH_2), 14.0 (–CH_3). Anal. Calc. for $C_{32}H_{29}N_3$: C, 84.36; H, 6.42; N, 9.22. Found: C, 84.33; H, 6.17; N, 9.13%.

4.2.3. Synthesis of 4-{p-[N,N′-bis(tert-butoxycarbonyl)-N′-(phenyl)] phenylenediamino}-phenyl-6-phenyl-2,2′-bipyridine

4-(*p*-Bromophenyl)-6-phenyl-2,2′-bipyridine (1.40 g, 3.62 mmol), *N*′-(*tert*-butoxycarbonyl)-*N*′-(phenyl)-*p*-phenylenediamine (1.24 g, 4.35 mmol), palladium acetate (18.0 mg, 0.080 mmol) and DPEphos (62.2 mg, 0.115 mmol) were charged into a flask and purged with argon. THF (20 ml) was added and NaOBu^t (0.81 g, 8.43 mmol) was added in one portion. The reaction mixture was refluxed with stirring for about 20 h (as monitored by thin layer chromatography). After this period, the heat was temporarily removed, and 4-DMAP (74.0 mg, 0.60 mmol), THF (20 mL), and a 1.0 M solution of $(BOC)_2O$ (10.0 mmol) in THF (10 mL) were added. The reaction mixture was refluxed for 24 h. The solvent was removed by rotary evaporation. The residue was dissolved in dichloromethane, washed with distilled water, and dried over anhydrous sodium sulfate and concentrated. White powder was obtained by column chromatography [neutral Al_2O_3, PE:CH_2Cl_2 = 5:1 (V/V) containing 5% (V) triethylamine]: 1.8 g (yield: 72%). M.p.: 187–188 °C. ^{1}H NMR (300 MHz, $CDCl_3$): δ 8.73–8.68 (m, 2H), 8.63 (s, 1H), 8.20 (d, J = 7.0 Hz, 2H), 7.96 (s, 1H), 7.87 (t, J = 9.0 Hz, 1H), 7.77(d, J = 8.6 Hz, 2H), 7.56–7.46 (m, 3H), 7.37–7.29 (m, 5H), 7.23–7.19 (m, 7H, Ar), 1.48 (s, 9H, –C(CH_3)$_3$), 1.45 (s, 9H, –C(CH_3)$_3$). ^{13}C NMR (75 MHz, $CDCl_3$): δ 157.7, 154.1(*C*=O), 154.0 (*C*=O), 150.0, 144.2, 143.2, 141.1, 140.3, 139.7, 136.0, 129.6, 129.2, 128.0, 127.7, 127.5, 126.2, 124.4, 122.3, 118.9, 118.0 (Ar), 82.0 (–*C*(CH$_3$)$_3$), 81.7 (–*C*(CH$_3$)$_3$), 28.6 (–*C*H$_3$). Anal. Calc. for $C_{44}H_{42}N_4O_4$: C, 76.50; H, 6.13; N, 8.11. Found: C, 76.72; H, 5.85; N, 8.21%.

4.2.4. Synthesis of ligand H**L³**

4-{*p*-[*N*,*N*′-bis(*tert*-Butoxycarbonyl)-*N*′-(phenyl)]phenylenediamino}phenyl-6-phenyl-2,2′-bipyridine (1.39 g, 2.0 mmol) was placed in a flask under Ar. The system was heated to 185 °C for 12 h. Then the system was cooled to room temperature. THF (40 mL) was added to dissolve the solid. NaH (1.92 g, >52%, in mineral oil) was added and purged with argon. The reaction mixture was stirred for 1 h at room temperature, and then 1-bromobutane (1.5 mL, 14 mmol) was added dropwise via syringe. After the solution was refluxed until the conversion was complete (as monitored by thin layer chromatography), it was poured into ice-water mixture and extracted with CH_2Cl_2 until the water phase was colorless. The combined organic solutions were washed with distilled water, and dried over anhydrous sodium sulfate and concentrated. The residue was separated by column chromatography [neutral Al_2O_3, PE:CH_2Cl_2 = 8:1 (V/V) containing 5% (V) triethylaminine]. H**L³** was obtained as pale green crystal by recrystallizing from MeOH/EA solution: 0.97 g (yield: 81%). M.p.: 124–125 °C. ^{1}H NMR (300 MHz, $CDCl_3$): δ 8.72–8.66 (m, 2H), 8.62 (s, 1H), 8.19 (d, J = 8.5 Hz, 2H), 7.95 (s, 1H), 7.86 (t, J = 8.6 Hz, 1H), 7.71(s, broad, 2H), 7.55–7.44 (m, 3H), 7.35–7.27 (m, 3H), 7.01–6.91 (m, broad, 9H, Ar), 3.70 (s, broad, 4H, α (–CH_2)), 1.69 (s, broad, 4H, β (–CH_2)), 1.40 (s, broad, 4H, γ (–CH_2)), 0.97 (m, 3H, –CH_3). ^{13}C NMR (75 MHz, $CDCl_3$): δ 156.9, 156.6, 156.0, 149.8, 148.9, 144.8, 140.4, 139.9, 136.8, 129.3, 128.8, 128.6, 127.8, 127.3, 127.0, 126.8, 123.6, 122.1, 121.5, 120.9, 120.5, 117.3, 116.4, 115.7 (Ar), 52.2 (α-CH_2), 29.7 (β-CH_2), 20.3 (γ-CH_2), 14.0 (–CH_3). Anal. Calc. for $C_{42}H_{42}N_4$: C, 83.68; H, 7.02; N, 9.29. Found: C, 83.93; H, 6.83; N, 9.07%.

4.3. Synthesis of Pt(II) complexes

Complexes [(**L**^{1})PtCl] (**1a**) and [(**L**^{1})PtC≡CC_6H_5] (**2a**) were synthesized according to the literature method [34,35].

4.3.1. General procedure for the synthesis of **1b** and **1c**

A mixture of H**L²** or H**L³** (0.5 mmol), K_2PtCl_4 (0.5 mmol) and glacial acetic acid (50 mL) was refluxed for 12 h under a nitrogen atmosphere in the absence of light. The reaction mixture was then cooled to room temperature and filtered. The obtained solid was recrystallized from MeOH/CH_2Cl_2 solution to form desired product.

4.3.2. Synthesis of [(**L²**)PtCl] (**1b**)

1b was obtained as red crystal: 0.32 g (yield: 92%). ^{1}H NMR (300 MHz, $CDCl_3$): δ 8.91 (d, J = 4.3 Hz, 1H), 8.72 (d, J = 8.1 Hz, 1H), 8.43 (s, 1H), 8.36 (t, J = 8.6 Hz, 1H), 8.16 (s, 1H), 7.99 (d, J = 8.9 Hz, 2H), 7.90 (t, J = 6.4 Hz, 1H), 7.78 (d, J = 8.6 Hz, 1H), 7.51–7.41 (m, 3H), 7.26–7.06 (m, 5H), 6.92 (d, J = 8.9 Hz, 2H, Ar), 3.80 (t, J = 7.5 Hz, 2H, α (–CH_2)), 1.61 (m, 2H, β (–CH_2)), 1.37 (m, 2H, γ (–CH_2)), 0.91 (t, J = 7.3 Hz, 3H, –CH_3). ^{13}C NMR(75 MHz, $CDCl_3$): δ 166.4, 157.8, 154.4, 151.0, 150.6, 149.2, 147.1, 142.6, 139.3, 135.6, 131.2, 130.2, 128.3, 128.1, 127.4, 126.3, 125.3, 124.3, 124.2, 122.7, 116.5, 115.2, 115.1 (Ar), 52.7 (α-CH_2), 29.9 (β-CH_2), 20.7 (γ-CH_2), 14.3 (–CH_3). Anal. Calc. for $C_{32}H_{28}ClN_3Pt$: C, 56.10; H, 4.12; N, 6.13. Found: C, 56.15; H, 3.88; N, 5.89%.

4.3.3. Synthesis of [(**L³**)PtCl] (**1c**)

1c was obtained as red crystal: 0.35 g (yield: 84%). ^{1}H NMR (300 MHz, $CDCl_3$): δ 8.91 (d, J = 5.2 Hz, 1H), 8.70 (d, J = 8.0 Hz, 1H), 8.41 (s, 1H), 8.36 (t, J = 8.0 Hz, 1H), 8.14 (s, 1H), 7.97 (d,

J = 8.6 Hz, 2H), 7.90 (t, J = 6.5 Hz, 1H), 7.77 (d, J = 7.4 Hz, 1H), 7.49 (d, J = 7.3 Hz, 1H), 7.31 (m, 3H), 7.16–7.08 (m, 4H), 7.04–6.96 (m, 5H), 6.82 (d, J = 8.6 Hz, 2H, Ar), 3.71 (m, 4H, α (–CH_2)), 1.60 (m, 4H, β (–CH_2)), 1.37 (m, 4H, γ (–CH_2)), 0.92 (m, 6H, –CH_3). ^{13}C NMR (75 MHz, $CDCl_3$): δ 165.0, 157.0, 153.6, 150.4, 149.9, 147.9, 146.7, 145.7, 142.3, 139.2, 138.5, 134.8, 130.1, 129.4, 127.9, 127.7, 126.4, 124.7, 123.6, 123.4, 122.8, 121.6, 121.2, 114.9, 114.6, 113.9 (Ar), 52.3 (α-CH_2), 29.6 (β-CH_2), 20.3 (γ-CH_2), 14.0 (–CH_3). Anal. Calc. for $C_{42}H_{41}ClN_4Pt$: C, 60.61; H, 4.97; N, 6.73. Found: C, 60.91; H, 4.60; N, 6.59%.

*4.3.4. General procedure for the synthesis of **2b** and **2c***

A mixture of **1b** or **1c** (0.30 mmol), RC≡CH (1 mmol), Et_3N (5 mL) and CuI (5 mg) in degassed CH_2Cl_2 (50 mL) was stirred for 12 h under a nitrogen atmosphere at room temperature in the absence of light. The reaction mixture was then evaporated to dryness under reduced pressure. The crude product was purified by flash chromatography (neutral Al_2O_3, CH_2Cl_2 as eluent) and recrystallized from CH_2Cl_2/MeOH solution.

*4.3.5. Synthesis of [(**L**^{2})PtC≡CC_6H_5] (**2b**)*

Complex **2b** was obtained as orange needles (0.18 g, 81%). ^{1}H NMR (300 MHz, $CDCl_3$): δ 9.06 (d, J = 5.3 Hz, 1H), 8.71 (d, J = 8.1 Hz, 1H), 8.48 (s, 1H), 8.37 (t, J = 8.6 Hz, 1H), 8.22 (s, 1H), 7.99 (d, J = 8.9 Hz, 2H), 7.86–7.75 (m, 3H), 7.46–7.31 (m, 4H), 7.31–7.22 (m, 4H), 7.20–6.95 (m, 4H), 6.93 (d, J = 8.9 Hz, 2H, Ar), 3.80 (t, J = 7.6 Hz, 2H, α (–CH_2)), 1.62 (m, 2H, β (–CH_2)), 1.38 (m, 2H, γ (–CH_2)), 0.91 (t, J = 7.4 Hz, 3H, –CH_3); ^{13}C NMR (75 MHz, $CDCl_3$): δ 165.1, 158.6, 154.6, 151.7, 151.3, 150.4, 147.1, 142.6, 138.9, 138.7, 132.2, 131.3, 130.2, 128.4, 128.2, 127.4, 126.9, 126.2, 125.3, 125.2, 124.4, 123.8, 123.1, 116.6, 115.4, 115.0 (Ar), 52.6 (α-CH_2), 30.0 (β-CH_2), 20.7 (γ-CH_2), 14.3 (–CH_3). Anal. Calc. for $C_{40}H_{33}N_3Pt$: C, 63.99; H, 4.43; N, 5.60. Found: C, 63.92; H, 4.32; N, 5.53%.

*4.3.6. Synthesis of [(**L**^{3})PtC≡CC_6H_5] (**2c**)*

Complex **2c** was obtained as deep red crystal (0.23 g, 87%). ^{1}H NMR (300 MHz, $CDCl_3$): δ 9.05 (d, J = 5.3 Hz, 1H), 8.69 (d, J = 8.1 Hz, 1H), 8.45 (s, 1H), 8.36 (t, J = 8.6 Hz, 1H), 8.18 (s, 1H), 7.96 (d, J = 8.9 Hz, 2H), 7.87–7.74 (m, 3H), 7.39–7.26 (m, 6H), 7.16–6.95 (m, 10H), 6.83 (d, J = 9.0 Hz, 2H, Ar), 3.72 (m, 4H, α (–CH_2)), 1.59 (m, 4H, β (–CH_2)), 1.39 (m, 4H, (γ-CH_2)), 0.92 (m, 6H, –CH_3). ^{13}C NMR (75 MHz, $CDCl_3$): δ 164.3, 158.0, 154.0, 151.0, 150.7, 150.4, 147.9, 147.1, 145.7, 142.3, 139.2, 138.4, 138.2, 131.8, 130.7, 129.4, 129.2, 127.9, 127.8, 127.7, 126.7, 125.2, 124.8, 123.9, 123.2, 122.9, 121.7, 121.1, 114.9, 114.6, 114.2 (Ar), 52.3 (α-CH_2), 29.6 (β-CH_2), 20.3 (γ-CH_2), 14.0 (–CH_3). Anal. Calc. for $C_{50}H_{46}N_4Pt$: C, 66.87; H, 5.16; N, 6.24. Found: C, 66.95; H, 4.97; N, 6.02%.

5. X-ray crystallography

The intensity data were collected with the ω scan mode (187 K) on a Bruker Smart APEX diffractometer with CCD detector using Mo Kα radiation (λ = 0.71073 Å). Lorentz, polarization factors were made for the intensity data and absorption corrections were performed using SADABS program [59]. The crystal structures were solved using the SHELXTL program and refined using full matrix least squares [60]. The positions of hydrogen atoms were calculated theoretically and included in the final cycles of refinement in a riding model along with attached carbons except the disordered butyl and butyl aniline moieties.

C42H41ClN4Pt, MW = 832.33, red crystal, 0.25 × 0.20 × 0.06 mm^3, monoclinic, $P2(1)/c$, a = 17.3834(9), b = 13.0070(7), c = 16.4081(9) Å, β = 109.3840(10), V = 3499.7(3) Å^3, Z = 4, $D_{calcd.}$ = 1.580 g/cm^3, μ = 4.122 mm^{-1}, R_1/wR_2 [$I > 2\sigma(I)$]: 0.0655/0.1786. R_1/wR_2 [all reflections]: 0.0822/0.1885. S = 1.046. Residual electron density: 2.528 and −2.057 e Å^{-3}.

Supplementary material

CCDC 699169 contains the supplementary crystallographic data for this paper. These data can be obtained free of charge from The Cambridge Crystallographic Data Centre via www.ccdc.cam.ac.uk/data_request/cif.

Acknowledgments

This work is supported by the National Natural Science Foundation of China (No. 50673088), Science Fund for Creative Research Groups (No. 20621401) and 973 Project (2009CB623600).

References

[1] J.A.G. Williams, Top. Curr. Chem. 281 (2007) 205.
[2] P.-T. Chou, Y. Chi, Eur. J. Inorg. Chem. (2006) 3319.
[3] P.-T. Chou, Y. Chi, Chem. Eur. J. 13 (2007) 380.
[4] J.-L. Chen, S.-Y. Chang, Y. Chi, K. Chen, Y.-M. Cheng, C.-W. Lin, G.-H. Lee, P.-T. Chou, C.-H. Wu, P.-I. Shih, C.-F. Shu, Chem. Asian J. 3 (2008) 2112.
[5] W. Sun, H. Zhu, P.M. Barron, Chem. Mater. 18 (2006) 2602.
[6] B.-P. Yan, C.C.C. Cheung, S.C.F. Kui, H.-F. Xiang, V.A.L. Roy, S.-J. Xu, C.-M. Che, Adv. Mater. 19 (2007) 3599.
[7] B.-P. Yan, C.C.C. Cheung, S.C.F. Kui, V.A.L. Roy, C.-M. Che, S.-J. Xu, Appl. Phys. Lett. 91 (2007) 063508.
[8] K.-H. Wong, M.C.-W. Chan, C.-M. Che, Chem. Eur. J. 5 (1999) 2845.
[9] P.K.M. Siu, S.-W. Lai, W. Lu, N. Zhu, C.-M. Che, Eur. J. Inorg. Chem. (2003) 2749.
[10] Q.-Z. Yang, L.-Z. Wu, H. Zhang, B. Chen, Z.-X. Wu, L.-P. Zhang, C.-H. Tung, Inorg. Chem. 43 (2004) 5195.
[11] C.-M. Che, J.-L. Zhang, L.-R. Lin, Chem. Commum. (2002) 2556.
[12] W. Lu, V.A.L. Roy, C.-M. Che, Chem. Commun. (2006) 3972.
[13] C. Adachi, M.A. Baldo, S.R. Forrest, S. Lamansky, M.E. Thompson, R.C. Kwong, Appl. Phys. Lett. 78 (2001) 1622.
[14] V. Adamovich, J. Brooks, A. Tamayo, A.M. Alexander, P.I. Djurovich, B.W. D'Andrade, C. Adachi, S.R. Forrest, M.E. Thompson, New J. Chem. 26 (2002) 1171.
[15] B.W. D'Andrade, J. Brooks, V. Adamovich, M.E. Thompson, S.R. Forrest, Adv. Mater. 14 (2002) 1032.
[16] J. Brooks, Y. Babayan, S. Lamansky, P.I. Djurovich, I. Tsyba, R. Bau, M.E. Thompson, Inorg. Chem. 41 (2002) 3055.
[17] A.S. Ionkin, W.J. Marshall, Y. Wang, Organometallics 24 (2005) 619.
[18] W.-Y. Wong, Z. He, S.-K. So, K.-L. Tong, Z. Lin, Organometallics 24 (2005) 4079.
[19] B. Yin, F. Niemeyer, J.A.G. Williams, J. Jiang, A. Boucekkine, L. Toupet, H.L. Bozec, V. Guerchais, Inorg. Chem. 45 (2006) 8584.
[20] Z. He, W.-Y. Wong, X. Yu, H.-S. Kwok, Z. Lin, Inorg. Chem. 45 (2006) 10922.
[21] G.-J. Zhou, X.-Z. Wang, W.-Y. Wong, X.-M. Yu, H.-S. Kwok, Z. Lin, J. Organomet. Chem. 692 (2007) 3461.
[22] B. Hirani, J. Li, P.I. Djurovich, M. Yousufuddin, J. Oxgaard, P. Persson, S.R. Wilson, R. Bau, W.A. Goddard III, M.E. Thompson, Inorg. Chem. 46 (2007) 3865.
[23] D.J. Cárdenas, A.M. Echavarren, M.C.R. Arellano, Organometallics 18 (1999) 3337.
[24] J.A.G. Williams, A. Beeby, E.S. Davies, J.A. Weinstein, C. Wilson, Inorg. Chem. 42 (2003) 8609.
[25] W. Sotoyama, T. Satoh, N. Sawatari, H. Inoue, Appl. Phys. Lett. 86 (2005) 153505.
[26] S.J. Farley, D.L. Rochester, A.L. Thompson, J.A.K. Howard, J.A.G. Williams, Inorg. Chem. 44 (2005) 9690.
[27] M. Cocchi, D. Virgili, V. Fattori, D.L. Rochester, J.A.G. Williams, Adv. Funct. Mater. 17 (2007) 285.
[28] S.-W. Lai, M.C.-W. Chan, T.-C. Cheung, S.-M. Peng, C.-M. Che, Inorg. Chem. 38 (1999) 4046.
[29] C.-K. Koo, Y.-M. Ho, C.-F. Chow, M.H.-W. Lam, T.-C. Lau, W.-Y. Wong, Inorg. Chem. 46 (2007) 3603.
[30] W. Lu, M.C.W. Chan, K.-K. Cheung, C.-M. Che, Organometallics 20 (2001) 2477.
[31] V.W.-W. Yam, R.P.-L. Tang, K.M.-C. Wong, X.-X. Lu, K.-K. Cheung, N. Zhu, Chem. Eur. J. 8 (2002) 4066.
[32] S.C.F. Kui, S.S.-Y. Chui, C.-M. Che, N. Zhu, J. Am. Chem. Soc. 128 (2006) 8297.
[33] W. Lu, M.C.W. Chan, N. Zhu, C.-M. Che, C. Li, Z. Hui, J. Am. Chem. Soc. 126 (2004) 7639.
[34] W. Lu, B.-X. Mi, M.C.W. Chan, Z. Hui, N. Zhu, S.T. Lee, C.-M. Che, Chem. Commun. (2002) 206.
[35] W. Lu, B.-X. Mi, M.C.W. Chan, Z. Hui, C.-M. Che, N. Zhu, S.-T. Lee, J. Am. Chem. Soc. 126 (2004) 4958.
[36] S.C.F. Kui, I.H.T. Sham, C.C.C. Cheung, C.-W. Ma, B. Yan, N. Zhu, C.-M. Che, W.-F. Fu, Chem. Eur. J. 13 (2007) 417.
[37] U. Scherf, E.J.W. List, Adv. Mater. 14 (2002) 477.

[38] Y. Nishikitani, M. Kobayashi, S. Uchida, T. Kubo, Electrochim. Acta 46 (2001) 2035.
[39] P. Bonhôte, J.E. Moser, N. Valchopoulos, L. Walder, S.M. Zakeeruddin, R. Humphry-Baker, P. Péchy, M. Grätzel, Chem. Commun. (1996) 1163.
[40] G. Zhou, M. Baumgarten, K. Müllen, J. Am. Chem. Soc. 129 (2007) 12211.
[41] G. Zhou, N. Pschirer, J.C. Schöneboom, F. Eickemeyer, M. Baumgarten, K. Müllen, Chem. Mater. 20 (2008) 1808.
[42] F. Krönke, Synthesis 1 (1976) 1.
[43] J.P. Sadighi, R.A. Singer, S.L. Buchwald, J. Am. Chem. Soc. 120 (1998) 4960.
[44] D.S. Surry, S.L. Buchwald, Angew. Chem., Int. Ed. Engl. 47 (2008) 6338.
[45] V.H. Rawal, R.J. Jones, M.P. Cava, J. Org. Chem. 52 (1987) 19.
[46] S.-W. Lai, M.C.-W. Chan, K.-K. Cheung, C.-M. Che, Organometallics 18 (1999) 3327.
[47] J.H.K. Yip, Suwarno, J.J. Vittal, Inorg. Chem. 39 (2000) 3537.
[48] S.-W. Lai, H.-W. Lam, W. Lu, K.-K. Cheung, C.-M. Che, Organometallics 21 (2002) 226.
[49] A. Hofmann, L. Dahlenburg, R. van Eldik, Inorg. Chem. 42 (2003) 6528.
[50] K.M.-C. Wong, W.-S. Tang, X.-X. Lu, N. Zhu, V.W.-W. Yam, Inorg. Chem. 44 (2005) 1492.
[51] M.-Y. Chou, M.-K. Leung, Y.O. Su, C.L. Chiang, C.-C. Lin, J.-H. Liu, C.-K. Kuo, C.Y. Mou, Chem. Mater. 16 (2004) 651.
[52] F.E. Goodson, S.I. Hauck, J.F. Hartwig, J. Am. Chem. Soc. 121 (1999) 7527.
[53] R.M. Leasure, W. Ou, J.A. Moss, R.W. Linton, T.J. Meyer, Chem. Mater. 8 (1996) 173.
[54] R.P. Kingsborough, T.M. Swager, J. Am. Chem. Soc. 121 (1999) 8825.
[55] P.G. Pickup, J. Mater. Chem. 9 (1999) 1641.
[56] M.O. Wolf, Adv. Mater. 13 (2001) 545.
[57] J. Hjelm, R.W. Handel, A. Hagfeldt, E.C. Constable, C.E. Housecroft, R.J. Forster, Inorg. Chem. 44 (2005) 1073.
[58] R. Chen, B.C. Benicewicz, Macromolecules 36 (2003) 6333.
[59] R.H. Blessing, Acta Crystallogr. A 51 (1995) 33.
[60] G.M. Sheldrick, SHELXTL, Version 5.1, Bruker Analytical X-ray Systems, Inc., Madison, WI, 1997.